communications materials

Article

https://doi.org/10.1038/s43246-024-00574-5

Copper oxide coupled with photon upconversion for solar water splitting

Check for updates

Yerbolat Magazov[1,2], Vladislav Kudryashov[2], Kuanysh Moldabekov[1], Magzhan Amze[2], Aiisha Nurmanova[1], Asset Aliyev[1] & Nurxat Nuraje[1,2]

Photoelectrochemical water splitting is a promising solution for harnessing solar radiation for hydrogen production. Copper oxide semiconductors, particularly materials based on cuprous oxide, have attracted attention due to their abundant elemental availability and scalable synthesis methods. To improve the generated photocurrent of the photoelectrode system, photon upconversion materials can be implemented into water-splitting devices. Here, we demonstrate the potential application of triplet-triplet annihilation-based upconversion in solar-assisted water splitting and highlight the significance of photonic designs to improve the light-harnessing properties of photoactive materials. The triplet-triplet annihilation mechanism is particularly suitable due to its efficient conversion at low photon intensity, namely under 1-sun illumination. Our results show that Cu_2O coupled with an upconverter outperforms bare Cu_2O by 56% in terms of produced photocurrent density. We construct a hybrid water-splitting device with an extended absorption range by utilizing a semi-transparent 600 nm Cu_2O film with a 5 nm Au underlayer.

Harnessing sunlight for the direct synthesis of chemical fuels holds significant promise, with a particular focus on the clean and high-energy-density fuel produced through photoelectrochemical (PEC) water splitting, namely hydrogen[1]. In the pursuit of simplifying energy conversion through a single device, PEC water-splitting cells combine sunlight capture and water electrolysis processes.

Despite extensive research over several decades[2–4], numerous challenges in materials science still need resolution to establish PEC water splitting as a practical and competitive approach for hydrogen production. Copper oxide semiconductors, specifically materials based on cuprous oxide (Cu_2O), have attracted considerable attention among a range of economically viable options due to their abundant elemental availability and scalable synthesis methods[5]. Considering this material as a strong candidate for water-splitting purposes, a lot of effort was put into the investigation of solid-state overlayers[6], heterojunction partners[7–9] and catalytic interfaces[10–12] to improve the generated photovoltage, photocurrent, and durability of the photoelectrode system. Nevertheless, the limited efficiency in utilizing solar energy remains a hindrance in photocatalysis, primarily due to the narrow absorption range typically exhibited by photocatalysts. There were attempts to increase the efficiency of light absorption by improving the crystal quality or controlling the surface morphology[13–17]. Yet, most of them absorb and utilize only ultraviolet (UV) and visible light. Taking into consideration that UV accounts for 9.3% ($\lambda < 400$ nm) and visible light is 54.1% ($400 < \lambda < 800$ nm), the rest 36.6% which accounts for infrared (IR) light ($\lambda > 800$ nm) results in significant losses of solar energy[18]. Therefore, one of the major goals of this work is harnessing and full use of solar energy, especially IR region.

The problem of harvesting the lost photons can be solved by implementing photon upconversion (UC) materials into a water-splitting device. Photon upconversion is the phenomenon in which two or more photons with lower energy are transformed into a single photon with higher energy[19]. Among all UC mechanisms, triplet-triplet annihilation-based upconversion (TTA-UC) is especially suitable for solar water splitting due to the advantage of efficient conversion at low photon intensity (excitation power)[20–22]. The complexity of achieving effective upconversion under non-concentrated AM1.5 G solar illumination becomes evident through simple theoretical calculations and experiments when employing Ln^{3+} ions[23,24].

This work highlights the potential application of TTA-based UC in solar-assisted water splitting and illustrates the significance of photonic designs in addition to nanointerface engineering to improve the light-harnessing property of photoactive material. Here, we have developed a device where a photocatalyst based on Cu_2O film absorbs light within the UV-visible range, while the remaining IR light is absorbed by the upconverter. Subsequently, the upconverter emits high-energy photons which in turn can be utilized by our photocatalyst. This strategy allows us to dramatically improve the light-harnessing properties of our photoelectrode by irradiating the photocatalyst from dual perspectives (front and back-side illumination).

[1]Department of Chemical and Materials Engineering, School of Engineering & Digital Science, Nazarbayev University, Astana, Kazakhstan. [2]Renewable Energy Lab, National Laboratory Astana, Nazarbayev University, Astana, Kazakhstan. e-mail: nurxat.nuraje@nu.edu.kz

Results and Discussion

Photoelectrochemical system based on Cu_2O Photocathodes

Electrodeposited Cu_2O film functions as the component that absorbs light, generating photogenerated electrons used for solar-assisted water splitting. Typically, transparent conducting oxide films (FTO) are employed as substrates in transparent electronic devices. The substrate's contact with Cu_2O plays a pivotal role in creating an ohmic junction for the collection of photogenerated holes. For example, Cu_2O and FTO contact doesn't perfectly form an ohmic junction but rather creates a Schottky barrier, hindering hole collection and negatively affecting the current-potential response[25]. Furthermore, the Cu_2O morphology when deposited on bare FTO differed notably, forming large Cu_2O crystals compared to the consistent, uniform, and dense growth on gold-coated substrates. Figure 1 illustrates this variation across substrates, where it seems that the Au substrate impacts both the electronic junction and the electrodeposited film quality. We theorized that thin Au layers might address these issues while retaining high transparency. As depicted in Fig. 1, sputtering with an equivalent dose of 5 nm Au formed an island-like coating on the FTO. Interestingly, Cu_2O's electrodeposition onto these Au-coated substrates yielded films similar to those on thicker Au layers (10 and 15 nm), unlike the large Cu_2O particles on bare FTO (Supplementary Fig. 1).

The effects of Au thickness on photoelectrochemical and optical properties are shown in Fig. 2a, b. All samples were treated the same in terms of deposition of Cu_2O, where a 60-minute experiment was performed to obtain approximately 600 nm of cuprous oxide layer. The only difference was the various Au underlayer thicknesses. As seen in Fig. 2b, the photocurrent does not change significantly upon increasing the thickness of the gold layer. The maximum photocurrent is approximately -0.35 mA·cm^{-2} for all three cases (5, 10, and 15 nm) with minor variations obtained at the applied potential of 0 V vs. RHE. The difference is visible when we increase

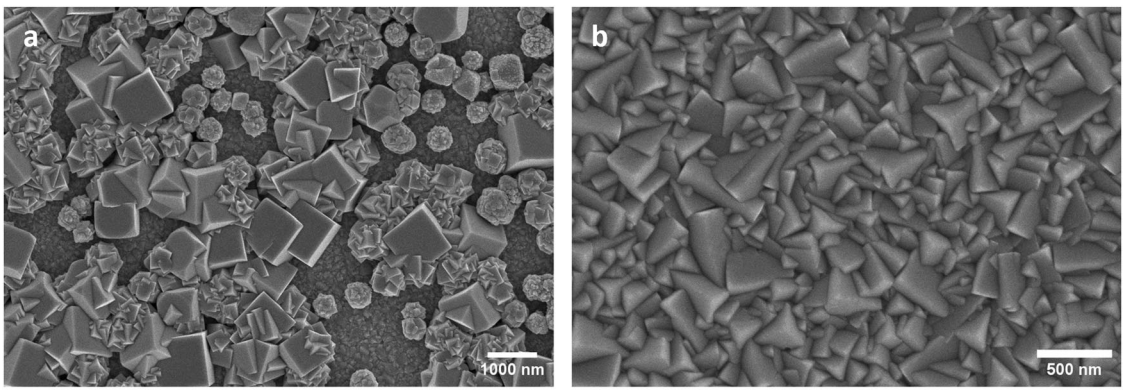

Fig. 1 | Scanning electron images of different substrates with identical treatments (60 min Cu_2O electrodeposition). **a** bare FTO glass, **b** FTO with a 5 nm Au film. Unlike on Au-treated surfaces, where Cu_2O develops uniformly and densely, on untreated FTO, it nucleates and grows into big, distinct crystals.

Fig. 2 | Effects of change in Au and Cu_2O thickness on photoelectrochemical and optical properties. **a** Transmittance spectrum of FTO substrates with varying amounts of sputtered Au. **b** Photoelectrochemical performance of 60 min electrodeposited Cu_2O on various Au-treated FTO substrates under 1-sun chopped illumination. **c** Photoelectrochemical performances and **d** IPCE spectra for Cu_2O films with different thicknesses deposited onto 5 nm Au-treated FTO substrates.

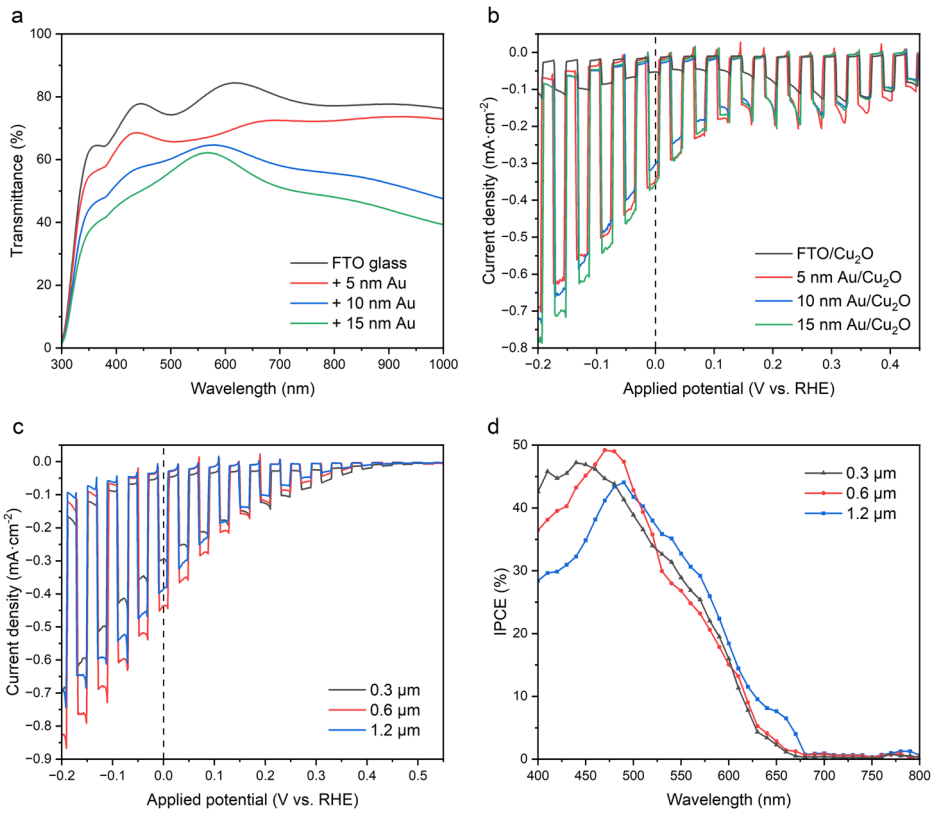

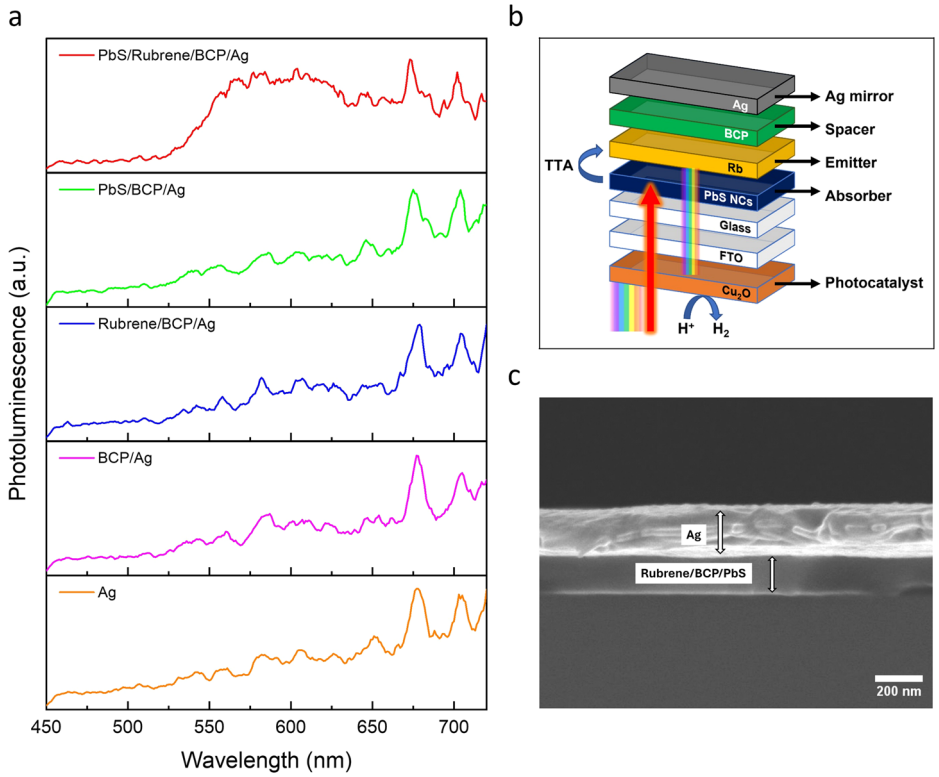

Fig. 3 | Performance of the assembled UC device. **a** Photoluminescence of UC device with control groups. Inset: control groups consist of the same components with the elimination of one or several elements. The devices were excited at 960 nm. **b** Schematic representation of UC device/Cu_2O configuration. **c** Cross-sectional scanning electron microscopy (SEM) image of assembled UC device on a silicon substrate.

the applied potential to a higher value, where the highest photocurrent was observed in ascending order of Au thickness, namely on a thicker layer of Au (-0.7 mA·cm^{-2}). In addition, the major distinction that draws our attention in this graph is the importance of the gold layer: as already mentioned earlier, Cu_2O and FTO contact doesn't perfectly form an ohmic junction which negatively affects the current-potential response.

The thickness of the Cu_2O photoactive layer is the next parameter to examine. Previous publications utilized Cu_2O films of 500 nm or larger[6,7,15]. Transparency was critical in our study, thus we investigated a range of Cu_2O thicknesses by altering the time of electrodeposition onto FTO substrates coated with 5 nm of Au. Three durations were investigated, with electrodepositions lasting 120, 60, and 30 minutes, generating film thicknesses of approximately 1200, 600, and 300 nm, respectively. The thickness of the films was measured by the profilometer (Dektak XT, Bruker). The photocathode performances of the devices varied, as shown in Fig. 2c, where the photoelectrode with the thinnest absorber layer (300 nm) demonstrated reduced photocurrents, whilst the 600 and 1200 nm films had virtually equal responses. The associated incident photon-to-current conversion efficiency (IPCE) is altered by variations in absorber thickness. According to Fig. 2d, the lower energy photons (~500−600 nm) are poorly absorbed by these Cu_2O films. For significant absorption in this range, film thicknesses of several micrometers are required[26] but for our configured tandem device, long-wavelength photon transmittance is an important factor.

Light penetration depth and carrier diffusion length are two key properties of semiconductors utilized either in photovoltaic or photoelectrochemical applications. The light penetration depth of Cu_2O at $\lambda = 600$ nm is approximately 2.2 μm[27]. The mobility of the charge carriers, which is heavily influenced by the synthesis procedure, determines the carrier diffusion length. For example, a single crystal or polycrystalline Cu_2O produced at high temperatures (thermal oxidation or sputtering) can attain a high carrier mobility of 100 cm^2·V^{-1}·s^{-1} [28,29]. Whereas the electrodeposition (a technique that was implemented in this work) produces tiny Cu_2O grains and carrier mobilities that rarely surpass 5 cm^2·V^{-1}·s^{-1} [30]. The carrier diffusion lengths obtained in high mobility Cu_2O systems (~100 cm^2·V^{-1}·s^{-1}) fall within the 1–10 μm range, which is in good agreement with the depth of light penetration[31]. High efficiencies are made possible in this situation by the ability to absorb almost all photons with energy higher than the bandgap. Lower mobility Cu_2O-based systems (>5 cm^2·V^{-1}·s^{-1}) result in charge carrier lengths much below 1 μm, which reduces the efficiency of the device by preventing the collection of longer wavelength (>600 nm) photons[32]. As a result, the 60-minute electrodeposition photocathode was chosen as a comparatively optimum choice for balancing PEC performance and optical transparency in the tandem water-splitting system.

UC/Cu_2O tandem device

UC devices typically consist of a material that absorbs low-energy photons, such as infrared light, and emits higher-energy photons in response. These devices can be integrated with solar water-splitting materials to increase the overall efficiency of the system. One example of such integration is illustrated in Fig. 3b, where PbS nanocrystals (NCs) absorb the low-energy photons, and by the TTA process, the rubrene and bathocuproine (BCP) allow to combine low-energy photons and produce the higher one (visible light). These high-energy photons are reflected by the silver mirror and get absorbed by the photocatalyst from the back side. Figure 3b displays a schematic illustration of the fully constructed tandem device composed of a Cu_2O photoactive layer and an upconversion device. In this configuration, the two systems are positioned in a back-to-back arrangement, namely our photocatalyst will be irradiated with visible light from dual perspectives (front and back-side illumination). A dual-absorber UC/Cu_2O tandem system utilizes photons from distinct parts of the solar spectrum in order to efficiently capture a wide range of sunlight.

Regarding the UC device itself, starting from the first layer, PbS NCs were deposited on the glass via the spin coating method in a nitrogen-filled glovebox. Without exposing it to air, the samples were loaded into a thermal evaporation instrument, where rubrene, BCP, and silver were deposited on top of PbS film, respectively. Figure 3b illustrates the layers consisting of PbS, rubrene, BCP, and Ag covered from both sides with glass and encapsulated with epoxy glue to prevent air and moisture contact. PbS nanocrystals absorb low-energy photons, namely at 960 nm (Supplementary Fig. 5), therefore, the device was illuminated with 960 nm incident light and upconverted

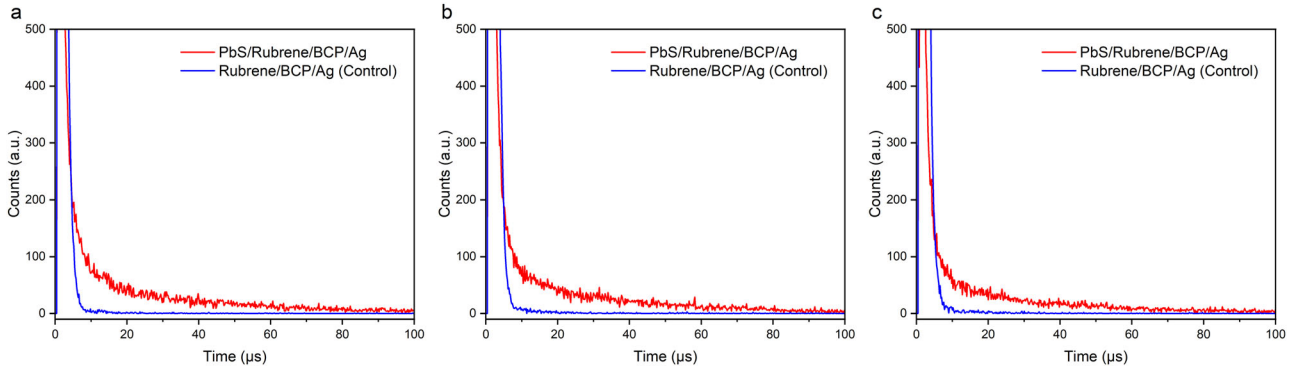

Fig. 4 | The luminescence decay kinetics of different emission wavelengths in the UC device (PbS/Rubrene/BCP/Ag) and control sample (Rubrene/BCP/Ag). Samples were excited with a picosecond 960 nm laser, and the decay of the emission was monitored at **a** 560 nm, **b** 580 nm, and **c** 610 nm.

photoluminescence (PL) was measured. Figure 3a and Fig. 4 display the upconverted photoluminescence (PL) intensity of the device at λ~550–625 nm. It was demonstrated that each component is crucial for obtaining the upconversion phenomenon since the elimination of one or several elements does not produce the same effect. It is possible to assume that two sharp peaks that appeared at 675 and 700 nm are due to the Ag mirror as those peaks appeared in all tested samples. Given that Cu_2O exhibits photoactivity within the visible spectrum up to 600 nm (Fig. 2d), the emitted photons from the UC device have a chance to get absorbed by this photoactive material.

We hypothesize that integrating upconversion device with Cu_2O photocathode would enhance the absorption ability of Cu_2O which in turn enhances the photoelectrochemical performance. The photoelectrochemical performance was measured by monitoring the photocurrent changes in the device. Figure 5a illustrates that Cu_2O coupled with an upconverter (UC) performs better than bare Cu_2O in terms of produced photocurrent density, namely bare Cu_2O produces $-0.32\ mA{\cdot}cm^{-2}$ at 0 V (vs. RHE) whereas Cu_2O/UC exhibits a peak at $-0.5\ mA{\cdot}cm^{-2}$ demonstrating an enhancement of 56%.

Relying on these statements and data, one can say that the observed effect may happen due to the presence of a thick silver layer that functions as a mirror. To eliminate such concerns, we fabricated the device consisting of Cu_2O and Ag by removing the upconversion part (PbS, Rubrene, BCP). As shown in Fig. 5a, the Ag does not affect the improved photocurrent meaning that our idea worked and confirmed. In addition, Fig. 5b shows the variations in spectrum response of the devices under monochromatic illumination as IPCE spectra. These two thin Cu_2O films use photons of higher energy (wavelengths shorter than 600 nm), as shown by an inflection in the IPCE spectra. The difference between these two devices is the response to the near IR region, where Cu_2O coupled with an upconversion device clearly utilizes the photons in this range. Figure 5d was constructed to accurately demonstrate the effect of upconversion on photocurrents produced by Cu_2O. It can be seen that under non-concentrated 950 nm illumination (LED source, $400\ \mu W{\cdot}cm^{-2}$) Cu_2O coupled with an upconversion device shows some photoresponse compared with bare Cu_2O. As for the photoactivity of photoelectrodes under visible light (LED source, 390–730 nm), no major difference was observed (Fig. 5c).

To demonstrate the enhanced performance of our device, Table 1 was constructed by compiling current reports of similar UC-PEC water-splitting systems based on Cu_2O. There are few documented works that use such configuration (Cu_2O/UC), and even when they do, they all rely on upconversion materials based on lanthanides. There are two primary limitations that affect the PEC efficiency of these systems. One issue is that the upconversion efficiency of near-infrared in rare earth-doped $NaYF_4$ is low, as these materials can only utilize specific wavelengths[33]. That is why photoelectrode systems listed in Table 1 illustrate the photoactivity using concentrated laser beams (mostly 980 nm). In one of the systems, namely $NaYF_4$:Yb–Er/AZO/Cu_2O, researchers tried to test under solar light (Xe lamp), however, no improvement in terms of photocurrent was observed. Another issue is that the high electrical resistance of $NaYF_4$, the near-infrared upconversion material employed in the PEC water-splitting system, creates a significant obstacle for the photo-carriers as they traverse the UC layer towards the conductive substrate. Consequently, this leads to a substantial decrease in the PEC water-splitting efficiency.

In our system, the two above-listed issues are eliminated. As can be seen in the main text, our device can operate under solar irradiation ($100\ mW{\cdot}cm^{-2}$) and even low-power near-infrared light sources, which is more applicable to real-world scenarios. In addition, since our upconversion device is constructed in a way that does not physically contact the conductive substrate and photocatalyst, it will not act as a barrier for charge carriers.

At this point, it should be mentioned that there are two limitations present in this work related to photocatalyst and upconversion devices. First, due to the focus on designing and optimizing the photoelectrode system to enhance the light-harvesting capability of Cu_2O, the improvements of the photocathode itself in terms of photocurrent and stability were neglected. Chemical instability (photocorrosion) and low photocurrents are common issues for the bare Cu_2O-based photocathodes which limit the measurement of hydrogen production and solar-to-hydrogen efficiency.

Second, due to the instability of the main material, it is difficult to estimate the stability of the upconversion device. As can be seen in Fig. 6, our fabricated upconversion device is stable for a prolonged time sitting on the bench under normal lab conditions (air atmosphere, room temperature) since it was encapsulated preventing air or moisture exposure. It should be mentioned that rubrene can undergo degradation when exposed to extended light, particularly ultraviolet (UV) radiation[34]. Nevertheless, due to the presence at the top of Cu_2O, which absorbs UV-visible light, the rubrene is shielded from photodegradation. Therefore, improvements in electrode stability and solar-to-hydrogen efficiency are anticipated in future works.

Conclusions

In conclusion, we used an infrared-to-visible photon upconversion device and photocathode based on Cu_2O film to fabricate a hybrid photoelectrochemical water-splitting system. In the process of creating such a device, we investigated how various elements of the device architecture (transparency and thickness of the layers) affect the performance. A hybrid water-splitting device with an extended absorption range was created by utilizing a semi-transparent photoelectrode. We determined that there is a 56% increase in the generated photocurrent density. Further improvements in electrode stability and solar-to-hydrogen efficiency are anticipated soon from investigations of suitable overlayers.

Methods

Fabrication of Cu_2O photocathode

Cuprous oxide films were electrodeposited onto fluorine-doped tin oxide (FTO) substrates. The FTO-glass substrates underwent a cleaning process

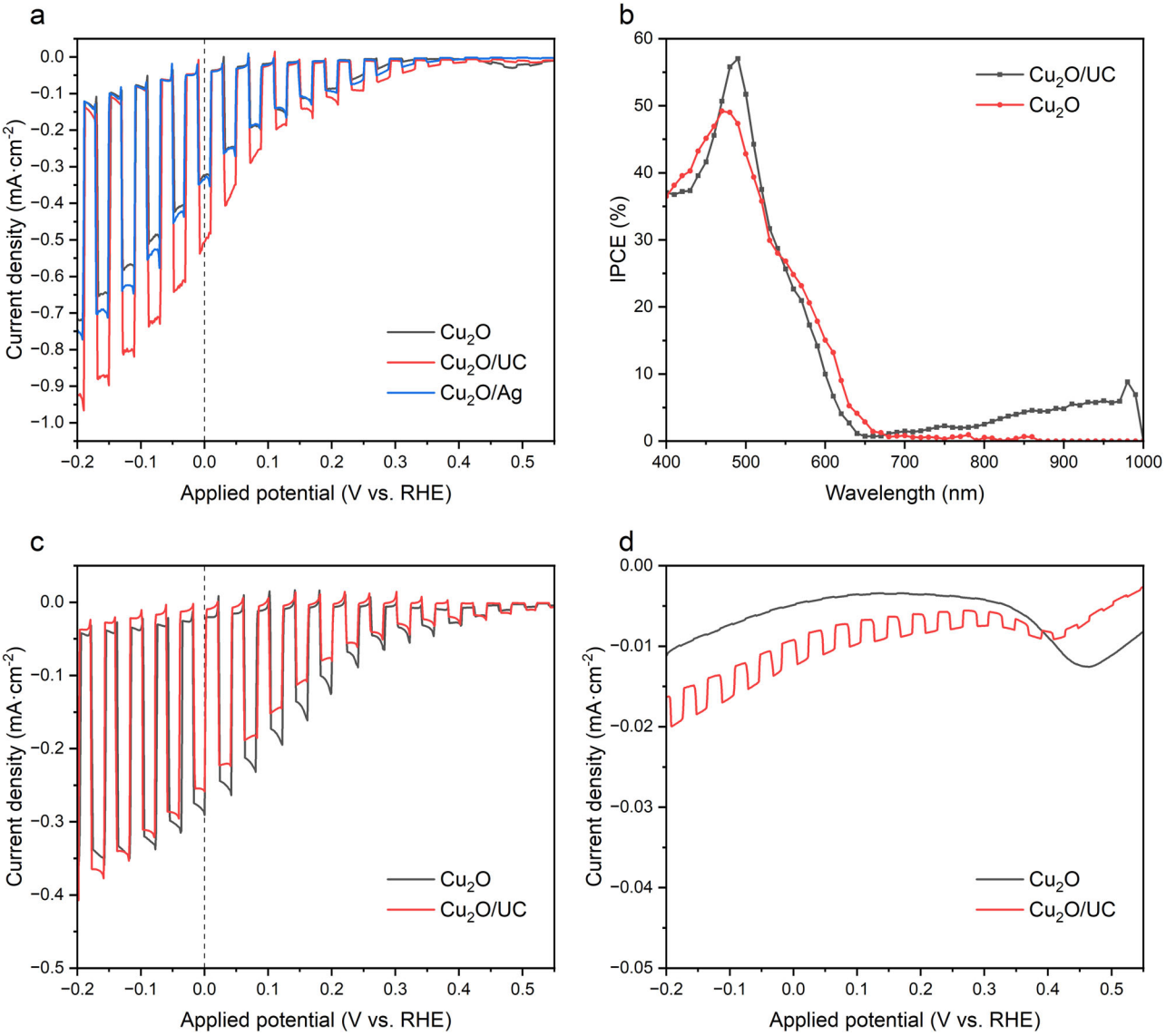

Fig. 5 | Photoelectrochemical effects of upconversion device. a Photocurrent responses and corresponding **b** IPCE of photocathodes, produced by 60 min electrodeposition of Cu_2O on 5 nm Au layer, tested in Na_2SO_4 (pH 6.4) electrolyte under 1-sun illumination. **c** Photocurrent responses of photocathodes under visible light. **d** photocurrent responses of photocathodes under IR light (950 nm).

Table 1 | The photocurrent performance of the NIR-light-driven PEC conversion systems based on Cu_2O photocatalyst

Photoelectrode	Light source	Electrolyte solution	Photocurrent density (at 0 V vs. RHE)	Photocurrent density of pristine Cu_2O (at 0 V vs. RHE)	Ref.
$NaYF_4$:Yb–Tm/Cu_2O	980 nm laser (1.0 W·cm^{-2})	0.1 M Na_2SO_4	0.04 mA·cm^{-2}	–	Jia et al.[37]
	NIR light (Xe lamp with 850 nm long-pass filter		0.0041 mA·cm^{-2}	0.0009 mA·cm^{-2}	
$NaYF_4$:Yb–Er/AZO/Cu_2O	980 nm laser (50 mW·cm^{-2})	0.1 M Na_2SO_4	0.07 mA·cm^{-2}	–	Chen et al.[38]
	980 nm laser (1 W·cm^{-2})		0.40 mA·cm^{-2}	–	
	980 nm laser (3 W·cm^{-2})		0.65 mA·cm^{-2}	–	
	1-sun (Xe lamp)		1 mA·cm^{-2}	1 mA·cm^{-2}	
NGF/$BiVO_4$/Cu_2O	980 nm laser (1.5 W·cm^{-2})	0.1 M Na_2SO_4	0.33 mA·cm^{-2}	0.008 mA·cm^{-2}	Ma et al.[39]
	550 nm (30 mW·cm^{-2})		0.0046 mA·cm^{-2}	0.002 mA·cm^{-2}	
Ag/BCP/Rubrene/PbS/Cu_2O	950 nm LED light (0.4 mW·cm^{-2})	0.5 M Na_2SO_4	0.003 mA·cm^{-2}	0 mA·cm^{-2}	This work
	1-sun (Xe lamp, 100 mW·cm^{-2})		0.5 mA·cm^{-2}	0.32 mA·cm^{-2}	

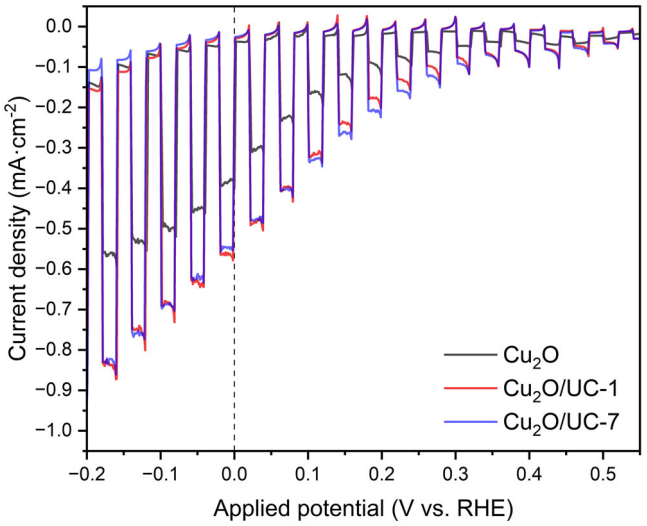

Fig. 6 | Photoelectrochemical effects of upconversion device. Photocurrent responses of photocathodes, produced by 60 min electrodeposition of Cu_2O on 5 nm Au layer, tested in Na_2SO_4 (pH 6.4) electrolyte under 1-sun illumination. *UC-1* (upconversion device tested 1 day after fabrication), *UC-7* (upconversion device tested 7 days after fabrication).

involving sequential ultrasonic treatments in Hellmanex III solution (15 min), deionized water (15 min), acetone (15 min), methanol (15 min), and isopropanol (15 min). Subsequently, Au coating was applied to the substrates through direct current (DC) sputtering. The semi-transparent Au treatments were monitored using quartz crystal microbalance (QCM) resulting in substrates with nominal thicknesses of 5, 10, and 15 nm. The electrodeposition of Cu_2O from a basic solution of lactate stabilized $CuSO_4$ followed a previously established procedure[6,12]. A constant current density of -0.1 mA·cm^{-2} was applied to Au-coated FTO-glass substrates using a two-electrode configuration with platinum serving as the counter electrode. The temperature of the bath solution was kept at 30 °C and the deposition time was varied (see the details in the main text).

Assembling of Cu_2O/UC device

PbS nanocrystals capped with oleic acid ligands were produced following a previously established procedure[35,36]. In brief, lead precursors were created by dissolving 11.380 g of lead acetate trihydrate in a mixture of 21 mL of oleic acid and 300 mL of 1-octadecene and degassing it at 100 °C overnight. The obtained solution was then heated to 120 °C under nitrogen, followed by the rapid injection of a mixture containing 3.15 mL of bis(trimethylsilyl)sulfide and 150 mL of 1-octadecene. After the synthesis, PbS nanocrystals were purified and extracted with acetone, butanol, and methanol, redispersed in octane, and stored as a concentrated stock solution.

An aliquot of PbS nanocrystals dissolved in octane, namely a 3 mg/mL solution was spin-coated on the glass side of the Cu_2O photocathode (back side of FTO) at 1500 rpm for 15 s in a nitrogen-filled glovebox. The samples were subsequently transferred into a thermal evaporator. With the base pressure below 1×10^{-6} Torr, 50 nm of rubrene, followed by 55 nm of bathocuproine (BCP), and finally, 200 nm of silver (Ag) were deposited on top of the PbS layer. Each device was encapsulated with a piece of glass using a light-curable epoxy (Osilla) in a glovebox.

Material characterization

The morphology of the substrates and photoelectrodes was characterized using a high-resolution scanning electron microscope (ZEISS Crossbeam 540). X-ray diffraction patterns were collected using a Rigaku SmartLab X-ray Diffractometer (XRD, Rigaku Corp., Tokyo, Japan) with a Cu Kα radiation source. XPS data were collected on NEXSA (Thermo Scientific) using a monochromatic Al Ka X-ray source (1486.6 eV). The transmittance spectra were collected using a UV–Vis–NIR spectrophotometer (Perkin Elmer, Lambda 1050).

The photoluminescence spectroscopy and the decay kinetics of long-lived luminescence were recorded with an FLS1000 spectrometer (Edinburgh Instr.) with UV, Vis, and NIR PMTs (Hamamatsu). The samples were photoexcited at $\lambda_{exc} = 960$ nm by a laser system based on an Nd:YAG laser (LQ529, Solar LS), an OPO (LP604, Solar LS), and a second harmonic generator (LG305, Solar LS).

Electrochemical characterization

The PEC performance was evaluated in a standard three-electrode configuration using the Cu_2O/UC device as the photocathode, a Pt wire as a counter electrode, and an Ag/AgCl reference electrode. 0.5 M aqueous solution of Na_2SO_4 was used as an electrolyte. PalmSens4 potentiostat/galvanostat (PalmSens BV, Netherlands) was used to acquire the photoresponse under chopped light irradiation from a 300 W Xe lamp (TLS260-300X, Newport, USA). The PEC cell was positioned for illumination at one-sun intensity calibrated with a reference silicon cell (Newport). In selected experiments, an LED lamp (Ossila Solar Simulator) was used to test the performance under visible and infrared light alone. The output power at a specific wavelength was measured with a Si sensor power meter (Thorlabs PM160). The scan rate for all current–potential measurements was 10 mV·s^{-1} in the cathodic direction. The recorded potentials, expressed as V vs. Ag/AgCl, were converted to the reversible hydrogen electrode (RHE) scale using the following equation:

$$E_{RHE} = E_{Ag/AgCl} + 0.059 \cdot pH + E^{\circ}_{Ag/AgCl}$$

where $E_{Ag/AgCl}$ is the recorded potential against the reference electrode and $E^{\circ}_{Ag/AgCl} = 0.1976$ V at 25 °C.

Data availability

The datasets generated during the current study are available from the corresponding author upon reasonable request. Supplementary information is available in the online version of the paper.

Received: 24 February 2024; Accepted: 12 July 2024;
Published online: 20 July 2024

References

1. Walter, M. G. et al. Solar water splitting cells. *Chem. Rev.* **110**, 6446–6473 (2010).
2. Memmino, R. Solar energy conversion by photoelectrochemical processes. *Electrochim. Acta* **25**, 77–88 (1980).
3. Bard, A. J. & Fox, M. A. Artificial photosynthesis: solar splitting of water to hydrogen and oxygen. *Acc. Chem. Res.* **28**, 141–145 (1995).
4. Grätzel, M. Photoelectrochemical cells. *Nature* **414**, 338–344 (2001).
5. Meyer, B. K. et al. Binary copper oxide semiconductors: From materials towards devices. *Phys. Status Solidi B Basic Res.* **249**, 1487–1509 (2012).
6. Paracchino, A. et al. Ultrathin films on copper(i) oxide water splitting photocathodes: A study on performance and stability. *Energy Environ. Sci.* **5**, 8673–8681 (2012).
7. Niu, W. et al. Extended Light Harvesting with Dual Cu_2O-Based Photocathodes for High Efficiency Water Splitting. *Adv. Energy Mater.* **8**, 1702323 (2018).
8. Siol, S. et al. Band Alignment Engineering at Cu_2O/ZnO Heterointerfaces. *ACS Appl. Mater. Interfaces* **8**, 21824–21831 (2016).
9. Afroz, K., Moniruddin, M., Bakranov, N., Kudaibergenov, S. & Nuraje, N. A heterojunction strategy to improve the visible light sensitive water splitting performance of photocatalytic materials. *J. Mater. Chem. A Mater.* **6**, 21696–21718 (2018).
10. Moniruddin, M. et al. Designing CdS-based ternary heterostructures consisting of Co-metal and CoOx cocatalysts for photocatalytic H_2 evolution under Visible Light. *Inorg. Chem.* **58**, 12325–12333 (2019).

11. Tilley, S. D., Schreier, M., Azevedo, J., Stefik, M. & Graetzel, M. Ruthenium oxide hydrogen evolution catalysis on composite cuprous oxide Water-splitting photocathodes. *Adv. Funct. Mater.* **24**, 303–311 (2014).
12. Morales-Guio, C. G., Tilley, S. D., Vrubel, H., Graẗzel, M. & Hu, X. Hydrogen evolution from a copper(I) oxide photocathode coated with an amorphous molybdenum sulphide catalyst. *Nat. Commun.* **5**, 3059 (2014).
13. Salehmin, M. N. I. et al. Highly photoactive Cu_2O nanowire film prepared with modified scalable synthesis method for enhanced photoelectrochemical performance. *Sol. Energy Mater. Sol. Cells* **182**, 237–245 (2018).
14. Luo, J. et al. Cu_2O nanowire photocathodes for efficient and durable solar water splitting. *Nano Lett.* **16**, 1848–1857 (2016).
15. Pan, L. et al. Boosting the performance of Cu_2O photocathodes for unassisted solar water splitting devices. *Nat. Catal.* **1**, 412–420 (2018).
16. Bai, J. et al. A novel 3D ZnO/Cu_2O nanowire photocathode material with highly efficient photoelectrocatalytic performance. *J. Mater. Chem. A Mater.* **3**, 22996–23002 (2015).
17. Hamdani, I. R. & Bhaskarwar, A. N. Cu_2O nanowires based p-n homojunction photocathode for improved current density and hydrogen generation through solar-water splitting. *Int J. Hydrog. Energy* **46**, 28064–28077 (2021).
18. Tao, F. (Feng), Schneider, W. F. & Kamat, P. V. *Heterogeneous Catalysis at Nanoscale for Energy Applications*. (Wiley, 2015).
19. Auzel, F. Upconversion and Anti-Stokes Processes with f and d Ions in Solids. *Chem. Rev*. **104**, 139–174 (2004).
20. Singh-Rachford, T. N. & Castellano, F. N. Photon upconversion based on sensitized triplet-triplet annihilation. *Coord. Chem. Rev*. **254**, 2560–2573 (2010).
21. Huang, Z. et al. Hybrid Molecule-Nanocrystal Photon Upconversion Across the Visible and Near-Infrared. *Nano Lett.* **15**, 5552–5557 (2015).
22. Huang, Z. et al. Enhanced Near-Infrared-to-Visible Upconversion by Synthetic Control of PbS Nanocrystal Triplet Photosensitizers. *J. Am. Chem. Soc.* **141**, 9769–9772 (2019).
23. Richards, B. S., Hudry, D., Busko, D., Turshatov, A. & Howard, I. A. Photon Upconversion for Photovoltaics and Photocatalysis: A Critical Review. *Chem. Rev*. **121**, 9165–9195 (2021).
24. Christiansen, J. et al. Analytical model for the intensity dependence of 1500 nm to 980 nm upconversion in Er 3+: A new tool for material characterization. *J. Appl. Phys.* **125**, (2019).
25. Dias, P. et al. Transparent Cuprous Oxide Photocathode Enabling a Stacked Tandem Cell for Unbiased Water Splitting. *Adv. Energy Mater*. **5**, 1501537 (2015).
26. Pavan, M. et al. TiO_2/Cu_2O all-oxide heterojunction solar cells produced by spray pyrolysis. *Sol. Energy Mater. Sol. Cells* **132**, 549–556 (2015).
27. Paracchino, A., Brauer, J. C., Moser, J. E., Thimsen, E. & Graetzel, M. Synthesis and characterization of high-photoactivity electrodeposited Cu_2O solar absorber by photoelectrochemistry and ultrafast spectroscopy. *J. Phys. Chem. C.* **116**, 7341–7350 (2012).
28. Minami, T., Nishi, Y. & Miyata, T. Heterojunction solar cell with 6% efficiency based on an n-type aluminum-gallium-oxide thin film and p-type sodium-doped Cu_2O sheet. *Appl. Phys. Express* **8**, 022301 (2015).
29. Minami, T., Nishi, Y. & Miyata, T. High-efficiency Cu_2O-based heterojunction solar cells fabricated using a Ga_2O_3 thin film as n-type layer. *Appl. Phys. Express* **6**, 044101 (2013).
30. Jeong, S. S., Mittiga, A., Salza, E., Masci, A. & Passerini, S. Electrodeposited ZnO/Cu_2O heterojunction solar cells. *Electrochim. Acta* **53**, 2226–2231 (2008).
31. Biccari, F., Malerba, C. & Mittiga, A. Chlorine doping of Cu_2O. *Sol. Energy Mater. Sol. Cells* **94**, 1947–1952 (2010).
32. Musselman, K. P., Marin, A., Schmidt-Mende, L. & MacManus-Driscoll, J. L. Incompatible length scales in nanostructured Cu_2O solar cells. *Adv. Funct. Mater.* **22**, 2202–2208 (2012).
33. Zhang, Q., Yang, F., Xu, Z., Chaker, M. & Ma, D. Are lanthanide-doped upconversion materials good candidates for photocatalysis? *Nanoscale Horiz.* **4**, 579–591 (2019).
34. Uttiya, S. et al. Stability to photo-oxidation of rubrene and fluorine-substituted rubrene. in. *Synth. Met.* **161**, 2603–2606 (2012).
35. Chang, L. Y., Lunt, R. R., Brown, P. R., Bulović, V. & Bawendi, M. G. Low-temperature solution-processed solar cells based on PbS colloidal quantum dot/CdS heterojunctions. *Nano Lett.* **13**, 994–999 (2013).
36. Zhao, N. et al. Colloidal PbS quantum dot solar cells with high fill factor. *ACS Nano* **4**, 3743–3752 (2010).
37. Jia, H. et al. Near-infrared light-induced photocurrent from a (NaYF4:Yb-Tm)/(Cu_2O) composite thin film. *Adv. Energy Mater.* **5**, 1401041 (2015).
38. Chen, X., Bu, Y., Li, H., Wang, X. & Ao, J. P. The fabrication of a photo-carrier transfer channel for a near infrared up-conversion coupled photocathode via a sandwich-like nanostructure. *J. Mater. Chem. C. Mater.* **9**, 8239–8248 (2021).
39. Ma, L. et al. Yb3+, Er3+ co-doped $NaGdF_4$/$BiVO_4$ embedded Cu_2O photocathodes for photoelectrochemical water reduction with near infrared light. *Appl. Surf. Sci.* **585**, 152650 (2022).

Acknowledgements

This work was supported by the Science Committee of the Ministry of Science and Higher Education of the Republic of Kazakhstan (Grant No. AP13068646 and Grant No. BR21882439). The authors are thankful to Dr. N. Ibayev, Dr. E. Seliverstova, and Dr. T. Serikov from Buketov Karaganda University for providing photo-luminescence spectroscopy data. Special thanks to Dr. Baurzhan Ilyassov from Astana IT University for helpful discussions and his valuable input in experimental design.

Author contributions

N.N. conceived and supervised the research project. Y.M. conceived the idea, conducted an experiment, interpreted the data, and wrote the manuscript. Y.M., K.M., and A.A. fabricated the electrodes and carried out PEC measurements. Y.M., M.A., A. N. fabricated the upconversion device and carried out PL measurements. Y.M. and V.K. conducted SEM, XRD, XPS, and UV-Vis experiments.

Competing interests

The authors declare no competing interests.

Additional information

Supplementary information The online version contains supplementary material available at https://doi.org/10.1038/s43246-024-00574-5.

Correspondence and requests for materials should be addressed to Nurxat Nuraje.

Peer review information *Communications Materials* thanks Jingshan Luo and the other, anonymous, reviewer(s) for their contribution to the peer review of this work. Primary Handling Editors: Jet-Sing Lee. A peer review file is available.